ARTICLE

doi:10.1038/nature14431

Neurotransmitter and psychostimulant recognition by the dopamine transporter

Kevin H. Wang[1]†*, Aravind Penmatsa[1]†* & Eric Gouaux[1,2]

Na^+/Cl^--coupled biogenic amine transporters are the primary targets of therapeutic and abused drugs, ranging from antidepressants to the psychostimulants cocaine and amphetamines, and to their cognate substrates. Here we determine X-ray crystal structures of the *Drosophila melanogaster* dopamine transporter (dDAT) bound to its substrate dopamine, a substrate analogue 3,4-dichlorophenethylamine, the psychostimulants D-amphetamine and methamphetamine, or to cocaine and cocaine analogues. All ligands bind to the central binding site, located approximately halfway across the membrane bilayer, in close proximity to bound sodium and chloride ions. The central binding site recognizes three chemically distinct classes of ligands via conformational changes that accommodate varying sizes and shapes, thus illustrating molecular principles that distinguish substrates from inhibitors in biogenic amine transporters.

Signals by the biogenic amine neurotransmitters—dopamine (DA)[1], serotonin[2] and noradrenaline[3]—at chemical synapses are terminated by the cognate neurotransmitter sodium symporters (NSSs)[4–7]. Biogenic amines play profound roles in the development and function of the nervous system, as well as in animal behaviour and activity; thus NSSs are central to normal neurophysiology and are the targets of a spectrum of therapeutic and illicit agents, from antidepressants and antianxiety medications to cocaine and amphetamines[8]. Experimental and computational studies have shown that the DA, serotonin (SERT) and noradrenaline (NET) transporters harbour a conserved structural fold[9,10], first seen in the structure of LeuT[11]. Owing to variations in amino acid sequences[12], however, the biogenic amine transporters possess distinct yet overlapping pharmacological 'fingerprints'[13].

The dopamine transporter (DAT)[14] removes DA from synaptic and perisynaptic spaces, thus extinguishing its action at G-protein coupled DA receptors. To drive the vectorial 'uphill' movement of extracellular DA into presynaptic cells, DAT couples substrate transport to pre-existing sodium and chloride transmembrane gradients. Congruent with the multifaceted roles of DA in the nervous system, perturbation of dopaminergic signalling by disruption of native DAT function has profound consequences[15–17]. On the one hand, the amphetamines, potent and widely abused psychostimulants, are DAT substrates that enhance synaptic levels of DA both by competing with DA transport by DAT and by inducing the release of DA from synaptic vesicles into the cytoplasm, from where DA is then effluxed through DAT into the synaptic space[18–24]. On the other hand, the *Erythroxylum coca* leaf-derived alkaloid, cocaine, as well as synthetic cocaine derivatives are competitive inhibitors of DAT and enhance extracellular DA concentrations by locking the transporter in a transport inactive conformation[14,25–27]. Widely prescribed antidepressants specifically inhibit serotonin and noradrenaline uptake and typically have weaker affinities towards DAT[28,29].

Mutagenesis, chemical modification, binding and transport studies have implicated the central or S1 binding site in DAT, akin to the leucine and tryptophan site in LeuT, as the binding site occupied by DA, amphetamines, cocaine and antidepressants[25,26,30]. Moreover, the X-ray structure of a transport-inactive *Drosophila melanogaster* DAT (dDAT) in complex with nortriptyline shows the antidepressant bound at the central site[9,31]. Nevertheless, none of these studies have visualized the binding of DA, amphetamine or cocaine to an active DAT, nor have they illuminated distinctions in ligand pose and transporter conformation between substrates and inhibitors. Here we present X-ray structures of dDAT with substrates DA, methamphetamine or D-amphetamine, with the DA analogue 3,4-dichlorophenethylamine (DCP), and with cocaine or cocaine analogues.

Resurrection of transport activity

The previously reported structure of the dDAT-nortriptyline complex exploited a transport-inactive variant with five thermostabilizing mutations ($dDAT_{cryst}$)[9]. We recovered transport function yet retained favourable crystallization properties by reverting three thermostabilizing mutations (V275A, V311A and G538L) to their wild-type identities and by shifting the deletion of extracellular loop 2 (EL2; Extended Data Fig. 1). This minimal functional construct, $dDAT_{mfc}$, has a melting temperature of 48 °C[32], exhibits DA transport with a K_M of 8.2 ± 2.3 μM and V_{max} of 2.4 ± 0.2 pmol min^{-1} per 10^6 cells, compared to wild-type dDAT ($dDAT_{wt}$) with a K_M of 2.1 ± 0.7 μM and V_{max} of 4.5 ± 0.4 pmol min^{-1} per 10^6 cells (s.e.m., Fig. 1a). The $dDAT_{mfc}$ construct binds nisoxetine with a K_d of 36 nM compared to a K_i of 5.6 nM for wild-type dDAT[31] (Extended Data Fig. 2).

The central binding site in DAT, NET and SERT can be divided to subsites A, B and C[29,33]. Subsites A and C are well conserved in dDAT versus human DAT (hDAT), whereas subsite B, a pocket sculpted by TMs (transmembrane helices) 3 and 8, differs from hDAT in that residues lining this pocket in dDAT are Asp121 and Ser426 (Extended Data Fig. 3). We introduced mutations D121G (TM3) and S426M (TM8) into the $dDAT_{cryst}$ and $dDAT_{mfc}$ constructs to mimic hDAT subsite B[33]. These mutations enhanced the affinities for nisoxetine, β-CFT (2β-carbomethoxy-3β-(4-fluorophenyl)tropane) and DCP (Extended Data Figs 2, 4). Although constructs harbouring subsite B substitutions improved crystallization propensity, transport activity was extinguished (Extended Data Fig. 3c). Nevertheless, structures bearing these mutations were solved in complexes with cocaine, β-CFT, RTI-55(2β-carbomethoxy-3β-(4-iodophenyl)tropane)

[1]Vollum Institute, Oregon Health & Science University, 3181 SW Sam Jackson Park Road, Portland, Oregon 97239, USA. [2]Howard Hughes Medical Institute, Oregon Health & Science University, 3181 SW Sam Jackson Park Road, Portland, Oregon 97239, USA. †Present addresses: Amgen, Division of Molecular Structure and Characterization, Cambridge, Massachusetts 02142, USA (K.H.W.) and Molecular Biophysics Unit, Indian Institute of Science, Bangalore 560012, India (A.P.).
*These authors contributed equally to this work.

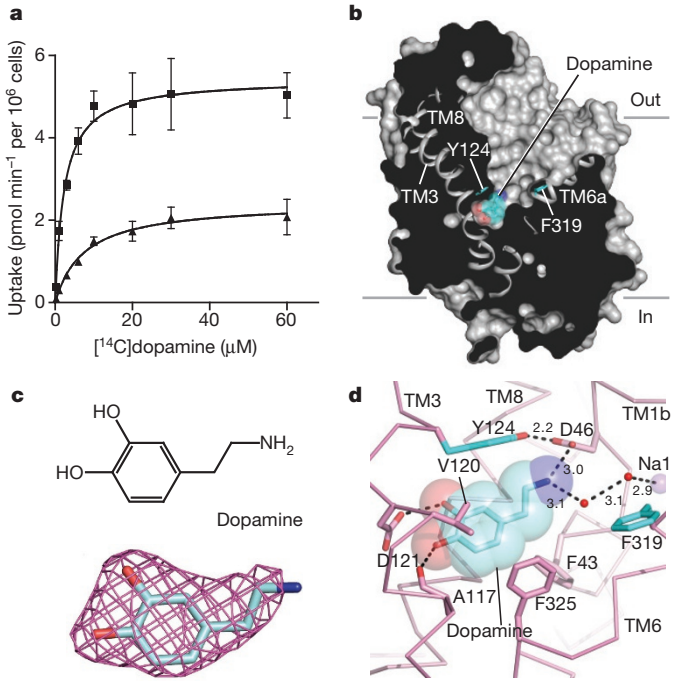

Figure 1 | Dopamine occupies central binding site. **a**, Michaelis–Menten plots of specific DA uptake by $dDAT_{wt}$ (squares) and $dDAT_{mfc}$ (triangles). Graph depicts one representative trial of two independent experiments. Error bars represent s.d. values for technical replicates measured in triplicate. **b**, Surface representation of the $dDAT_{mfc}$–DA complex viewed parallel to the membrane, with DA displayed as cyan spheres. Residues Y124 and F319 are shown as cyan sticks on the left and right sides of DA, respectively. **c**, Chemical structure and $F_o - F_c$ density for DA (3.0σ). **d**, Close-up view of DA in the binding pocket with hydrogen bonds shown as dashed lines. Sodium ions and water are shown as purple and red spheres, respectively.

or DCP (Supplementary Table 1). In the cocaine, RTI-55 and DCP complexes, superposition of structures with subsite B mutations onto structures of $dDAT_{mfc}$ complexes did not reveal prominent structural changes in the binding pocket or deviations in the positions of bound ligand (Extended Data Table 1).

Dopamine bound to central binding site

The structure of $dDAT_{mfc}$ bound to DA displays an outward-open conformation (Fig. 1b) where DA is situated in the central binding site, surrounded by TMs 1, 3, 6 and 8. The amine group points towards subsite A and interacts with the carboxylate of Asp46 at a distance of 3 Å. The catechol group occupies a subsite B cavity sculpted by Ala117, Val120, Asp121, Tyr124, Ser422 and Phe325 (Fig. 1c, d), residues predicted to interact with DA using homology models of DAT based on the substrate-bound occluded state of LeuT, analysis of uptake kinetics, and cysteine labelling studies[10,25,26,34]. Despite a lack of steric interference from DA, Phe319, which is equivalent to Phe253 in LeuT (in which it occludes solvent access to the LeuT binding pocket), remains splayed away from DA, in an orientation seen in the nortriptyline-bound structure[9,11].

The location and interactions of DA with dDAT recall predictions made through homology models of hDAT, although discrepancies between the cocrystal structure and the homology models are also evident. Site-directed mutagenesis and molecular dynamics simulations pointed to the crucial role of Asp46 (Asp79 in hDAT) in the recognition of DA[10,25,34,35], a residue conserved amongst biogenic amine neurotransmitters. GAT (γ-amino butyric acid transporter), GlyT (glycine transporter), and LeuT contain glycine at the equivalent position owing to the presence of a compensatory carboxylate group in the substrates[11]. One notable difference between the $dDAT_{mfc}$–DA structure and previous hDAT models, however, is a rotation in the χ1 torsion angle of ~130° in the side chain of Asp46 to maintain a 3 Å distance to the amine group of DA. This rotation severs the indirect coordination between Asp46 and the sodium ion at site 1 as observed in the nortriptyline–$dDAT_{cryst}$ complex[9]. Unlike previous simulation studies where DA binds in a dehydrated pocket[34], we observed non-protein electron density 3.1 Å from the amine group of DA, into which a water molecule was modelled. This water molecule forms a hydrogen bond with the water molecule that coordinates the sodium ion at site 1, resulting in a molecular network that links DA to the ion-binding sites. In the case of LeuT, substrate interaction with sodium site 1 is direct, with the carboxylate of leucine coordinating the sodium ion[11].

The catechol ring of DA interacts with TMs 3 and 8 by hydrogen bonds with the carboxylate group of Asp121 (Fig. 1d). Modelling studies predicted that DA occupies multiple poses within the binding pocket with the *meta*-hydroxyl either interacting with residues in TM8 equivalent to Ser421 or to Ser422 (dDAT numbering)[34]. By contrast, in the structure of $dDAT_{mfc}$–DA, the *para*-hydroxyl group interacts with both the carbonyl oxygen of Ala117 and the carboxylate of Asp121 at distances of 2.8 and 3.1 Å, respectively, whereas the *meta*-hydroxyl group interacts with the side chain of Asp121 at a distance of 2.7 Å and faces Ser422 in TM8 at a distance of 3.8 Å.

The residues poised to interact with the catechol ring vary across DAT orthologues with invertebrate DAT orthologues retaining alanine and aspartate at positions equivalent to residues 117 and 121, respectively, whereas in most mammalian DATs residue Asp121 is replaced by glycine and Ala117 by serine[9], the latter of which could act as a surrogate hydrogen bond partner for the catechol group. With hNET, the equivalent residues at 117 and 121 are Ala and Gly, raising the possibility of the catechol group of noradrenaline interacting with the hydroxyl of Ser420 in hNET (TM8; equivalent to Ser422 of dDAT and Ala423 in hDAT). We propose that these compensatory variations within subsite B dictate catecholamine recognition common to both DAT and NET. To explain why NET binds noradrenaline and DA with nearly equal apparent affinity yet DAT prefers DA[31], we must invoke longer-range, indirect interactions, perhaps involving subsite B and the non-helical TM6a–6b 'linker' because the 'Phe-box' surrounding the β-carbon position is conserved between NET and DAT.

Recognition of D-amphetamine and methamphetamine

To understand how amphetamines are transported by DAT despite lacking the hydroxyl groups of the catecholamines, we characterized the interactions between amphetamines and dDAT by binding assays and crystallographic studies. (+)-methamphetamine displaces [^{3}H]nisoxetine binding to $dDAT_{mfc}$ with a K_i value of 31 μM, whereas D-amphetamine, which lacks the *N*-methyl group present in methamphetamine, has a K_i of 86 μM (Fig. 2a). D-amphetamine is 10 to 100-fold weaker in its ability to inhibit DA transport in the dDAT compared to its mammalian counterparts[31]. The weaker affinities of dDAT for amphetamines compared to mammalian DATs may be due in part to differences in residues of subsite B. Indeed, the presence of Asp121 and Ser426 in invertebrate DATs creates a polar environment that does not complement the non polar benzyl groups of amphetamines (Fig. 1d). In mammalian DATs both methamphetamine (K_i = 0.5 μM) and D-amphetamine (K_i = 0.6 μM) are nearly as effective as cocaine (0.2 μM) at inhibition of DA uptake[36]. Although the maximal rate of transport (V_{max}) for D-amphetamine in hDAT is fivefold lower than for DA, the K_M values range from 0.8 to 2 μM[22], consistent with the notion that mammalian subsite B is more complementary towards the binding of amphetamines than subsite B in invertebrate DATs.

The structures of (+)-methamphetamine–$dDAT_{mfc}$ and D-amphetamine–$dDAT_{mfc}$ displayed outward open conformations with electron densities for the drugs found in the central binding site (Extended Data Fig. 5; Fig. 2b). The amine groups of methamphetamine

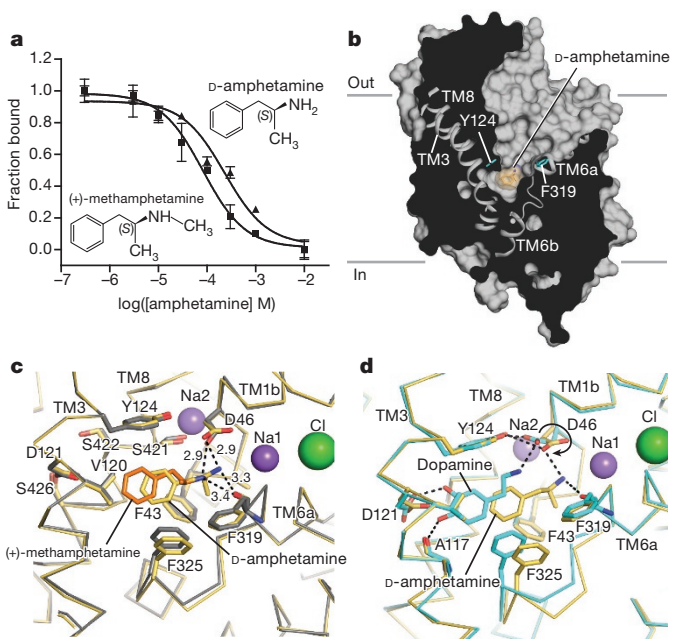

Figure 2 | Amphetamines bind to central site. **a**, Displacement of bound [^{3}H]nisoxetine by methamphetamine (K_i = 31 μM; squares) and D-amphetamine (K_i = 86 μM; triangles). Graph depicts one representative trial of two independent experiments. Error bars represent s.e.m. values for technical replicates measured in triplicate. **b**, Surface representation of D-amphetamine–dDAT$_{mfc}$ complex viewed parallel to the membrane with ligands shown as a light orange sphere. Residues Y124 and F319 are shown as cyan sticks on the left and right sides of DA, respectively. **c**, **d**, Superposition of binding pockets of the D-amphetamine–dDAT$_{mfc}$ structure in pale orange with binding pockets of methamphetamine–dDAT$_{mfc}$ (**c**, drug in orange, backbone in grey) and DA–dDAT$_{mfc}$ in teal (**d**). Hydrogen bond interactions are represented as dashed lines. Asp46 undergoes a χ1 torsion angle shift from −168° in DA-bound state to +62° in the D-amphetamine–dDAT$_{mfc}$.

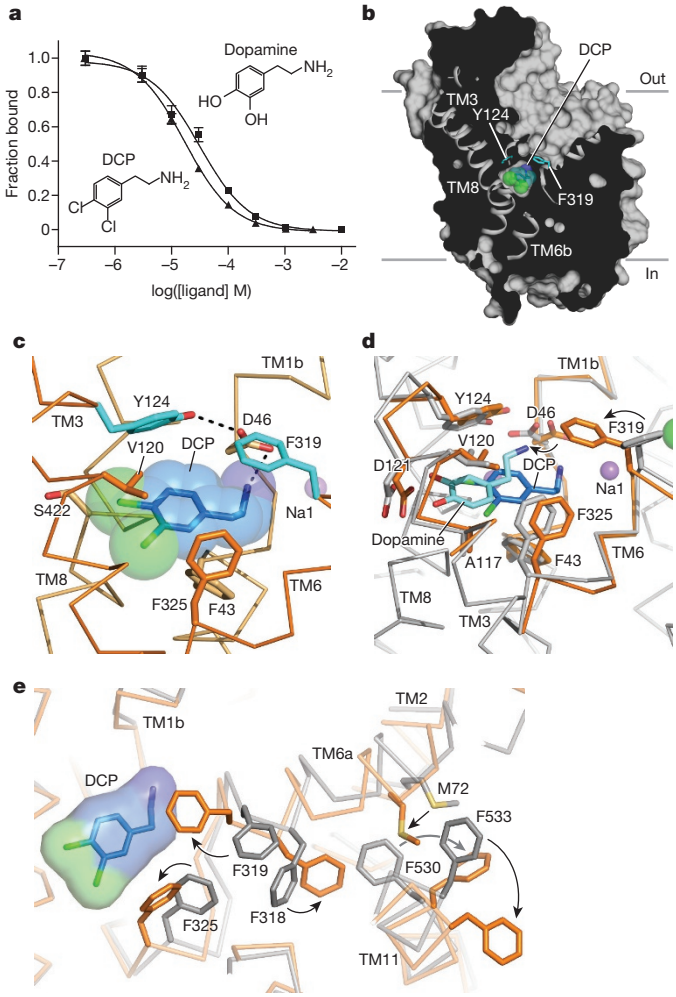

Figure 3 | DCP induces partial occlusion of central site. **a**, DCP and DA inhibit binding of [^{3}H]nisoxetine to dDAT$_{mfc}$ with K_i constants of 4.5 and 8.3 μM, respectively. Graph depicts one representative trial of two independent experiments, and data points indicate average values of technical replicates measured in triplicate for DA (squares) and DCP (triangles). Error bars represent s.d. values for individual data points measured in triplicate. **b**, Surface representation of the DCP–dDAT$_{mfc}$ complex viewed parallel to the membrane with DCP shown as blue spheres and chloride in green. Residues Y124 and F319 are shown as cyan sticks on the left and right sides of DCP, respectively. **c**, Close-up view of DCP in the binding pocket showing the hydrogen bond between the primary amine of DCP and D46 with a distance of 3.2 Å. Sodium ions are shown as purple spheres. **d**, Superposition of DA- and DCP-bound dDAT$_{mfc}$ structures reveals a 3.1 Å displacement in ligand position. The DA–dDAT$_{mfc}$ and DCP–dDAT$_{mfc}$ structures are coloured grey and orange, respectively. **e**, Conformational changes of phenylalanine side chain positions in the partially occluded state of DCP–dDAT$_{mfc}$ compared to the outward open state of nortriptyline–dDAT$_{cryst}$, coloured orange and grey, respectively.

and D-amphetamine lie closer to Asp46 at subsite A with hydrogen bonding distances of 2.9 Å, and the main chain carbonyl of Phe319 is positioned nearby at 3.3 Å (Fig. 2c). The amine group of D-amphetamine interacts with Asp46, which does not undergo the rotameric shift as seen in the DA-bound structure because D-amphetamine is situated in the centre of the pocket and not displaced by 2.8 Å towards TMs 3 and 8 as seen with DA (Fig. 2d). By contrast with earlier findings[25], we do not observe a disruption of the hydrogen bond between Asp46 and Tyr124 despite Asp46 clearly forming a hydrogen bond with the primary amine of D-amphetamine. Phe325 retains edge-to-face aromatic interactions with the phenyl group of amphetamines by way of a contraction of the TM6a–6b linker in comparison to the DA-bound state. Amphetamines adopt poses in the central binding that allow for interactions between their amino and aromatic groups and transporter subsites, thus explaining how the sterically smaller amphetamines compete with DA and act as substrates despite the absence of catechol-like hydroxyl groups.

Dopamine analogue stabilizes partially occluded state

DA is prone to oxidation and thus we sought a stable analogue for crystallographic and biochemical studies. Multiple high-affinity biogenic amine transporter inhibitors harbour halogen groups on the aromatic rings predicted to occupy subsite B[33,37] and thus we screened halogenated phenethylamine derivatives for binding to dDAT (Extended Data Fig. 4d). We discovered that 3,4-dichlorophenethylamine (DCP) possessed the greatest affinity and, because it is approximately isosteric to DA, was selected for further study (Fig. 3a).

One DCP molecule is lodged in the central binding pocket, with the amine group forming a hydrogen bond with Asp46, and the dichlorophenyl ring bordered by Val120 and Phe325 in subsites B and C, respectively (Fig. 3b–d, Extended Data Fig. 6). The position of DCP in the pocket is closer to that of D-amphetamine in dDAT and of substrate leucine in LeuT[11], whereas the position of DA is shifted towards TMs 3 and 8, probably owing to hydrogen bonding between the catechol hydroxyl groups and Asp121. As a result, the position of Asp46 in the DCP-bound structure is superimposable with the positions seen in the amphetamine-bound structures. Interestingly, the side chain of Phe319 rotates to occlude the binding pocket, a conformational change not seen in any of the inhibitor- or DA-bound structures (Fig. 3c, d). This rotamer of Phe319 prevents solvent access to the pocket, leaving an aperture only ~1 Å wide on the extracellular side of DCP. The equivalent residue in LeuT, Phe253, adopts the same

orientation in the occluded substrate-bound form, supporting the notion that the rearrangements seen in the DCP–dDAT$_{mfc}$ structure are on the pathway to a LeuT-like occluded state of dDAT[11]. Unlike the DA-bound state, there is no evidence of a water molecule associated with DCP in the structures, suggesting that formation of an occluded state is associated with dehydration of the binding pocket (Fig. 3c, d), similar to LeuT.

The partially occluded binding pocket of the DCP–dDAT$_{mfc}$ structure primarily results from rotations of TM1b and 6a 'into' the binding pocket, towards scaffold helices 3 and 8 and around axes centred near the non helical regions of TMs 1b and 6a (Extended Data Fig. 6a, c). In LeuT, studies of the transporter in solution and in the crystal show that TMs 1b and 6a, along with EL4, undergo conformational changes to close the extracellular gate[11,38,39]. Comparisons with the outward-open nortriptyline-bound state of dDAT[9] and the occluded state of LeuT indicate that, although the DCP ligand is nearly inaccessible to the extracellular solution, the inward rotations of TMs 1b (5.6°) and 6a (~7°) are less pronounced in dDAT than in LeuT[11] (Extended Data Fig. 6f, g). Nevertheless, these helical rotations position the side chain of Phe319 over the extracellular face of the binding pocket, and are associated with a series of phenylalanine side chain reorientations (Fig. 3e). TM11 undergoes an outward movement of 6° to accommodate these side chain shifts, and an inward movement of 5° is observed in TM2 (Extended Data Fig. 6b, d). Interestingly, TMs 2, 7 and 11 at the inner leaflet of the plasma membrane form a second cholesterol binding site (site 2) where a density for cholesteryl hemisuccinate (CHS) was observed in all the reported structures. Indeed, CHS enhances dDAT inhibitor affinity and we speculate that, in native membranes, cholesterol binds to sites 1 and 2, perhaps stabilizing DAT in an outward-open state (Extended Data Fig. 7)[39–41].

The occluded state is a Michaelis–Menten-like transport intermediate for LeuT and related transporters such as BetP, Mhp1 and MhsT[42–44] when bound to substrate. Disparities in conformations observed between LeuT and dDAT in the presence of substrate, however, may reflect bona fide differences that are dependent on the relative stabilities of distinct substrate-bound states. Nevertheless, we cannot exclude crystal lattice effects, Fab binding, lipid, or solutes present in the crystallization solutions that may favour the outward-open conformation observed for the dDAT–substrate complexes reported here.

Cocaine binds in the central site

The structure of the dDAT$_{mfc}$–cocaine complex exhibits an outward-open conformation (Fig. 4a) with cocaine bound to the central pocket at a site overlapping the nortriptyline site[45], adjacent to the Na1 and Na2 sodium ions and the chloride ion. The tertiary amino group of cocaine forms a salt bridge with Asp46 (TM1b) (Fig. 4b). We observe that the TM6a–6b linker contracts, allowing Phe325 to form edge-to-face aromatic interactions with the benzyl ring of cocaine (Fig. 4c).

The negative electrostatic potential of subsite B in dDAT compared to mammalian DATs probably underlies the reduced affinity of dDAT for cocaine. Altering this charged pocket to mimic mammalian DATs with the mutations D121G and S426M yielded a dDAT construct with enhanced binding affinities for cocaine and β-CFT, but not for RTI-55 (Fig. 4d, Extended Data Fig. 4a, b). We speculate that the carboxylate group of Asp121 does not form favourable interactions with the 4-fluorophenyl and 4-iodophenyl groups of β-CFT and RTI-55, respectively, perhaps accounting for some of the discrepancies in relative binding affinities between hDAT and dDAT.

Ligand docking studies using a homology model of DAT, in combination with biochemical binding assays and ligand-dependent disulphide trapping experiments, have probed the orientation of cocaine in the central binding site[25,26,30]. These studies predicted that the fluorophenyl moiety of β-CFT forms a hydrogen bond with the side chain equivalent to Asn125 in dDAT. Furthermore, the methyl ester of cocaine was thought to displace the side chain of Tyr124 to

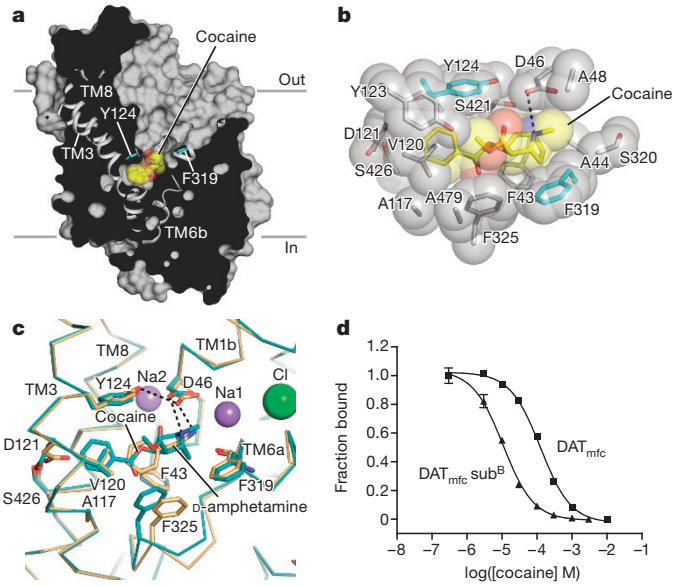

Figure 4 | Multivalent binding of cocaine. **a**, Surface representation of the structure of cocaine–dDAT$_{mfc}$ viewed parallel to the membrane, with cocaine displayed as yellow spheres. Residues Y124 and F319 are shown as cyan sticks on the left and right sides of cocaine, respectively. **b**, Close-up view of cocaine in the binding pocket with residues interfacing with cocaine shown as spheres. The tertiary amine of cocaine is 3.4 Å from the carboxylate of D46. **c**, Superposition of the binding pocket of the D-amphetamine–dDAT$_{mfc}$ structure in pale orange with the binding pocket of the cocaine–dDAT$_{mfc}$ structure in teal. **d**, Displacement of [^{3}H]nisoxetine by cocaine for dDAT$_{mfc}$ (squares) and dDAT$_{mfc}$ sub^{B} (triangles) constructs with inhibition constant (K_i) values of 33 ± 3 μM and 3 ± 0.3 μM, respectively. Graph depicts one representative trial of two independent experiments, and data points indicate average values of technical replicates measured in triplicate.

abrogate the hydrogen bond between Tyr124 and Asp46 as a mechanism of inhibiting transporter function. The dDAT$_{mfc}$–cocaine structure contradicts the finding that cocaine disrupts the Asp46–Tyr124 interaction and does not place the side chain of Asn125 in a location where it could interact with the fluorophenyl group of β-CFT.

To validate the cocaine-bound structure and conclusively identify residues that interact with tropane-based ligands, structures of dDAT were solved in the presence of the cocaine analogues β-CFT and RTI-55. Anomalous scattering by the iodide of RTI-55 corroborated the location and placement of the aromatic moiety of cocaine proximal to TMs 3 and 8 (Extended Data Fig. 8a). The $F_o - F_c$ 'omit' electron density maps for cocaine, β-CFT, and RTI-55 are consistent with the methyl ester group protruding into the base of the extracellular vestibule without disrupting the Asp46–Tyr124 interaction (Extended Data Figs 5, 8b). The position of β-CFT places the fluoro group 6 Å from the amide nitrogen of Asn125, indicating that Asn125 does not directly participate in binding of β-CFT. Superpositions of the cocaine–dDAT$_{mfc}$, β-CFT–dDAT$_{cryst}$, and RTI-55–dDAT$_{mfc}$ structures exhibited overall mean root-mean-square deviation (r.m.s.d.) values below 0.7 Å, and residues that make close contacts with the ligands overlap nearly entirely, indicating that the halide-substituted phenyl groups of β-CFT and RTI-55 do not markedly affect the architecture of the binding pocket (Extended Data Table 1).

Residues in the binding pocket that interact with cocaine are shared by β-CFT and RTI-55, with slight deviations in subsite B owing to the presence of halide substituents on these latter two inhibitors. At the distal end of the ligand, the halophenyl rings of β-CFT and RTI-55 or the benzoate of cocaine form van der Waals interactions primarily with Ala117, Val120, Tyr124, Phe325 and Ser422, all of which

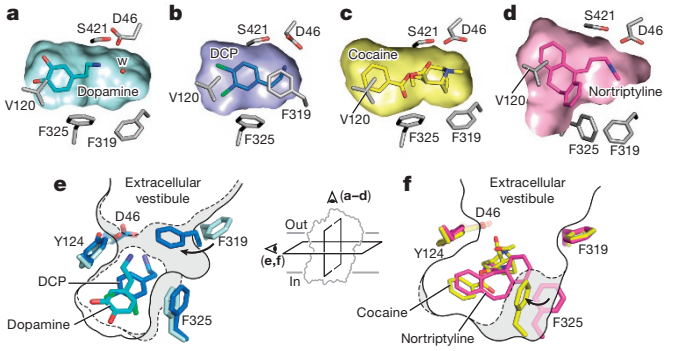

Figure 5 | Plasticity confers versatile recognition. **a**–**d**, Transverse sections of the binding pocket of $dDAT_{mfc}$ are shown as surface representations in the DA- (**a**), DCP- (**b**), cocaine- (**c**) and nortriptyline-bound (**d**) structures. A water molecule (W) is observed in the vicinity of DA in **a**. **e**, **f**, Schematic representing plasticity within the substrate and drug binding pockets in occluded state of DCP–$dDAT_{mfc}$ (broken lines) with DA–$dDAT_{mfc}$ (solid line) (**e**) and cocaine–$dDAT_{mfc}$ (broken lines) with nortriptyline–$dDAT_{cryst}$ (**f**, grey, PDB ID 4M48) (solid line). Inset represents schematic to show field of view for **a**–**d** and **e**, **f**.

were previously predicted to interact with these tropane-based inhibitors[25,46,47] (Fig. 4b). A comparison with the antidepressant nortriptyline–$dDAT_{cryst}$ structure[9] reveals that the smaller benzoate group of cocaine is accommodated with a shift of the TM6a–6b linker and a rotation of Phe325 into the binding pocket, which was not previously predicted. The tropane rings of cocaine, β-CFT and RTI-55 are bordered by Phe43, Ala44, Asp46, Ala48, Phe319 and Ser421. The side chain of Phe319 maintains a similar orientation as seen in the dDAT–nortriptyline structure owing to the bulky tropane ring and the methyl ester group present in all three tropane inhibitors. Overall, the docking and photolabelling studies predicted the location and orientation of cocaine and its analogues to overlap with the DA-binding site of DAT[25,26,30]. Our structures validate these findings yet indicate distinctions that have implications for the mechanism of inhibition by tropane ligands. Taken together, structures of dDAT in complex with tropane ligands suggest that inhibition is achieved by combining a free amine with bulky tropane and aromatic moieties to limit conformational movements of the transporter.

Plasticity of the substrate binding pocket

The inhibitor- and substrate-bound structures of dDAT indicate that the binding pocket of dDAT accommodates ligands of varying sizes largely by adjusting the orientation of the discontinuous region of TM6 and the side chains of Phe319 and Phe325 (Fig. 5; Extended Data Table 2a). Ligand recognition by dDAT is bipartite and requires an amine group that interacts with the carbonyl oxygens of Phe43 and Phe319 or the carboxylate of Asp46 in subsite A, in combination with an aromatic group that is stabilized by van der Waals interactions with residues lining a hydrophobic cleft formed by TMs 3, 6, and 8 of subsite B. The substrates DA, D-amphetamine, and methamphetamine each contain one phenyl ring linked to an ethylamine chain, requiring Phe325 to rotate inward to contract the size of the pocket and maintain edge-to-face aromatic interactions with these ligands (Extended Data Fig. 8c, Fig. 5a, e). In the DCP–$dDAT_{mfc}$ structure, Phe319 also rotates inward to cover the ligand, and similar to LeuT, this reorientation of Phe319 is required for the formation of the occluded state (Extended Data Fig. 8d, Fig. 5b, e). In order for Phe319 to cover DCP in the pocket, rotation of Phe319 is accompanied by the inward tilting of TM6a to bring the hinge region of TM6 towards the ligand (Extended Data Fig. 6). Accommodation of the single phenyl rings in tropane inhibitors requires Phe325 to assume a position similar to that seen in the DA-bound structure to provide edge-to-face aromatic interactions (Fig. 5c, f). To enlarge the binding pocket for multiple aromatic rings, the side chains of Phe319 and Phe325 are splayed outward as seen in the antidepressant-bound structures (Fig. 5d, f).

These structures provide a molecular explanation for the distinction between substrates and inhibitors of biogenic amine transporters. Substrates such as DA and amphetamines contain amine and aromatic functional groups at opposing ends of the molecule that interact with both the extracellular gate of TMs 1b and 6a and the scaffold TMs 3 and 8. In contrast, inhibitors exploit the flexibility of the binding pocket to bind to the outward open transporter with high affinity, acting like wedges to lock the transporter in an outward-open conformation. Tropane ligands achieve inhibition by inserting benzyl or halo-phenyl groups into the cavity of subsite B, with the tropane ring oriented to sterically hinder the movement of the extracellular gate. Antidepressants, like nortriptyline, differ from tropane inhibitors by coupling bulky aromatic moieties with an amine group to block conformational flexibility in the transporter.

Conclusions

Structures of dDAT in complex with both substrates and inhibitors emphasize the role of subsites in the pocket of dDAT in defining ligand specificity, a concept that can be expanded to understand variation in pharmacological profiles between biogenic amine transporters[33]. The DA-bound structure suggests that interactions between the catechol ring and subsite B, together with hydrogen bonding between the amine group of DA and Asp46, drive closure of the extracellular gates TMs 1b and 6a to form the occluded state. D-amphetamine and methamphetamine are bound in a manner distinct from DA in the pocket, and the absence of hydroxyl groups in amphetamines indicates that hydrophobic interactions must be sufficient for amphetamines to interact with subsite B residues and bridge the scaffold TMs 3 and 8 with the extracellular gating helices. The conformations of the DA, amphetamine and DCP-bound complexes probably represent snapshots following substrate and ion binding but before full closure of the extracellular gate, rather than the occluded conformation seen in LeuT bound to its substrates[11,48,49]. Questions extending from the substrate-bound structures involve the conformational changes required for DAT to transition to other states of the transport cycle and the roles of subsites A and B in neurotransmitter transport by mammalian DATs. Furthermore, the inhibitor-bound structures of dDAT provide a scaffold for addressing the mechanistic distinction between addictive and non-reinforcing analogues of cocaine[25,45,50].

Online Content Methods, along with any additional Extended Data display items, are available in the online version of the paper; references unique to these sections appear only in the online paper.

Received 6 November 2014; accepted 23 March 2015.
Published online 11 May 2015.

1. Carlsson, A., Lindqvist, M. & Magnusson, T. 3,4-Dihydroxyphenylalanine and 5-hydroxytryptophan as reserpine antagonists. *Nature* **180,** 1200 (1957).
2. Twarog, B. M. & Page, I. H. Serotonin content of some mammalian tissues and urine and a method for its determination. *Am. J. Physiol.* **175,** 157–161 (1953).
3. von Euler, U. Sympathin in adrenergic nerve fibres. *J. Physiol. (Lond.)* **105,** 26 (1946).
4. Hertting, G. & Axelrod, J. Fate of tritiated noradrenaline at the sympathetic nerve-endings. *Nature* **192,** 172–173 (1961).
5. Iversen, L. L. Role of transmitter uptake mechanisms in synaptic neurotransmission. *Br. J. Pharmacol.* **41,** 571–591 (1971).
6. Iversen, L. L. & Kravitz, E. A. Sodium dependence of transmitter uptake at adrenergic nerve terminals. *Mol. Pharmacol.* **2,** 360–362 (1966).
7. Kristensen, A. S. *et al.* SLC6 neurotransmitter transporters: structure, function, and regulation. *Pharmacol. Rev.* **63,** 585–640 (2011).
8. Pramod, A. B., Foster, J., Carvelli, L. & Henry, L. K. SLC6 transporters: structure, function, regulation, disease association and therapeutics. *Mol. Aspects Med.* **34,** 197–219 (2013).
9. Penmatsa, A., Wang, K. H. & Gouaux, E. X-ray structure of dopamine transporter elucidates antidepressant mechanism. *Nature* **503,** 85–90 (2013).
10. Koldsø, H., Christiansen, A. B., Sinning, S. & Schiøtt, B. Comparative modeling of the human monoamine transporters: similarities in substrate binding. *ACS Chem Neurosci* **4,** 295–309 (2013).

11. Yamashita, A., Singh, S. K., Kawate, T., Jin, Y. & Gouaux, E. Crystal structure of a bacterial homologue of Na^+/Cl^--dependent neurotransmitter transporters. *Nature* **437,** 215–223 (2005).
12. Beuming, T., Shi, L., Javitch, J. A. & Weinstein, H. A comprehensive structure-based alignment of prokaryotic and eukaryotic neurotransmitter/Na^+ symporters (NSS) aids in the use of the LeuT structure to probe NSS structure and function. *Mol. Pharmacol.* **70,** 1630–1642 (2006).
13. Gu, H., Wall, S. C. & Rudnick, G. Stable expression of biogenic amine transporters reveals differences in inhibitor sensitivity, kinetics, and ion dependence. *J. Biol. Chem.* **269,** 7124–7130 (1994).
14. Kilty, J. E., Lorang, D. & Amara, S. G. Cloning and expression of a cocaine-sensitive rat dopamine transporter. *Science* **254,** 578–579 (1991).
15. Kurian, M. A. *et al.* Homozygous loss-of-function mutations in the gene encoding the dopamine transporter are associated with infantile parkinsonism-dystonia. *J. Clin. Invest.* **119,** 1595–1603 (2009).
16. Giros, B., Jaber, M., Jones, S. R., Wightman, R. M. & Caron, M. G. Hyperlocomotion and indifference to cocaine and amphetamine in mice lacking the dopamine transporter. *Nature* **379,** 606–612 (1996).
17. Mergy, M. A. *et al.* The rare DAT coding variant Val559 perturbs DA neuron function, changes behavior, and alters *in vivo* responses to psychostimulants. *Proc. Natl Acad. Sci. USA* **111,** E4779–E4788 (2014).
18. Zaczek, R., Culp, S., Goldberg, H., McCann, D. J. & De Souza, E. B. Interactions of [3H]amphetamine with rat brain synaptosomes. I. Saturable sequestration. *J. Pharmacol. Exp. Ther.* **257,** 820–829 (1991).
19. Bönisch, H. The transport of (+)-amphetamine by the neuronal noradrenaline carrier. *Naunyn Schmiedebergs Arch. Pharmacol.* **327,** 267–272 (1984).
20. Eshleman, A. J., Henningsen, R. A., Neve, K. A. & Janowsky, A. Release of dopamine via the human transporter. *Mol. Pharmacol.* **45,** 312–316 (1994).
21. Goodwin, J. S. *et al.* Amphetamine and methamphetamine differentially affect dopamine transporters *in vitro* and *in vivo*. *J. Biol. Chem.* **284,** 2978–2989 (2009).
22. Sitte, H. H. *et al.* Carrier-mediated release, transport rates, and charge transfer induced by amphetamine, tyramine, and dopamine in mammalian cells transfected with the human dopamine transporter. *J. Neurochem.* **71,** 1289–1297 (1998).
23. Sonders, M. S., Zhu, S. J., Zahniser, N. R., Kavanaugh, M. P. & Amara, S. G. Multiple ionic conductances of the human dopamine transporter: the actions of dopamine and psychostimulants. *J. Neurosci.* **17,** 960–974 (1997).
24. Wall, S. C., Gu, H. & Rudnick, G. Biogenic amine flux mediated by cloned transporters stably expressed in cultured cell lines: amphetamine specificity for inhibition and efflux. *Mol. Pharmacol.* **47,** 544–550 (1995).
25. Beuming, T. *et al.* The binding sites for cocaine and dopamine in the dopamine transporter overlap. *Nature Neurosci.* **11,** 780–789 (2008).
26. Bisgaard, H. *et al.* The binding sites for benztropines and dopamine in the dopamine transporter overlap. *Neuropharmacology* **60,** 182–190 (2011).
27. Sørensen, G. *et al.* Neuropeptide Y Y5 receptor antagonism attenuates cocaine-induced effects in mice. *Psychopharmacology (Berl.)* **222,** 565–577 (2012).
28. Richelson, E. & Pfenning, M. Blockade by antidepressants and related compounds of biogenic amine uptake into rat brain synaptosomes: most antidepressants selectively block norepinephrine uptake. *Eur. J. Pharmacol.* **104,** 277–286 (1984).
29. Sørensen, L. *et al.* Interaction of antidepressants with the serotonin and norepinephrine transporters: mutational studies of the S1 substrate binding pocket. *J. Biol. Chem.* **287,** 43694–43707 (2012).
30. Dahal, R. A. *et al.* Computational and biochemical docking of the irreversible cocaine analog RTI 82 directly demonstrates ligand positioning in the dopamine transporter central substrate binding site. *J. Biol. Chem.* **289,** 29712–29727 (2014).
31. Pörzgen, P., Park, S. K., Hirsh, J., Sonders, M. S. & Amara, S. G. The antidepressant-sensitive dopamine transporter in *Drosophila melanogaster*: a primordial carrier for catecholamines. *Mol. Pharmacol.* **59,** 83–95 (2001).
32. Abdul-Hussein, S., Andrell, J. & Tate, C. G. Thermostabilisation of the serotonin transporter in a cocaine-bound conformation. *J. Mol. Biol.* **425,** 2198–2207 (2013).
33. Wang, H. *et al.* Structural basis for action by diverse antidepressants on biogenic amine transporters. *Nature* **503,** 141–145 (2013).
34. Huang, X. & Zhan, C. G. How dopamine transporter interacts with dopamine: insights from molecular modeling and simulation. *Biophys. J.* **93,** 3627–3639 (2007).
35. Kitayama, S. *et al.* Dopamine transporter site-directed mutations differentially alter substrate transport and cocaine binding. *Proc. Natl Acad. Sci. USA* **89,** 7782–7785 (1992).
36. Han, D. D. & Gu, H. H. Comparison of the monoamine transporters from human and mouse in their sensitivities to psychostimulant drugs. *BMC Pharmacol.* **6,** 6 (2006).
37. Newman, A. H., Zou, M. F., Ferrer, J. V. & Javitch, J. A. [3H]MFZ 2–12: a novel radioligand for the dopamine transporter. *Bioorg. Med. Chem. Lett.* **11,** 1659–1661 (2001).
38. Kazmier, K. *et al.* Conformational dynamics of ligand-dependent alternating access in LeuT. *Nature Struct. Mol. Biol.* **21,** 472–479 (2014).
39. Krishnamurthy, H. & Gouaux, E. X-ray structures of LeuT in substrate-free outward-open and apo inward-open states. *Nature* **481,** 469–474 (2012).
40. Hong, W. C. & Amara, S. G. Membrane cholesterol modulates the outward facing conformation of the dopamine transporter and alters cocaine binding. *J. Biol. Chem.* **285,** 32616–32626 (2010).
41. Zhao, Y. *et al.* Substrate-modulated gating dynamics in a Na^+-coupled neurotransmitter transporter homologue. *Nature* **474,** 109–113 (2011).
42. Malinauskaite, L. *et al.* A mechanism for intracellular release of Na^+ by neurotransmitter/sodium symporters. *Nature Struct. Mol. Biol.* **21,** 1006–1012 (2014).
43. Perez, C., Koshy, C., Yildiz, O. & Ziegler, C. Alternating-access mechanism in conformationally asymmetric trimers of the betaine transporter BetP. *Nature* **490,** 126–130 (2012).
44. Weyand, S. *et al.* Structure and molecular mechanism of a nucleobase-cation-symport-1 family transporter. *Science* **322,** 709–713 (2008).
45. Loland, C. J. *et al.* Relationship between conformational changes in the dopamine transporter and cocaine-like subjective effects of uptake inhibitors. *Mol. Pharmacol.* **73,** 813–823 (2008).
46. Lee, S. H. *et al.* Importance of valine at position 152 for the substrate transport and 2β-carbomethoxy-3β-(4-fluorophenyl)tropane binding of dopamine transporter. *Mol. Pharmacol.* **57,** 883–889 (2000).
47. Chen, J. G., Sachpatzidis, A. & Rudnick, G. The third transmembrane domain of the serotonin transporter contains residues associated with substrate and cocaine binding. *J. Biol. Chem.* **272,** 28321–28327 (1997).
48. Singh, S. K., Piscitelli, C. L., Yamashita, A. & Gouaux, E. A competitive inhibitor traps LeuT in an open-to-out conformation. *Science* **322,** 1655–1661 (2008).
49. Claxton, D. P. *et al.* Ion/substrate-dependent conformational dynamics of a bacterial homolog of neurotransmitter:sodium symporters. *Nature Struct. Mol. Biol.* **17,** 822–829 (2010).
50. Schmitt, K. C., Rothman, R. B. & Reith, M. E. Nonclassical pharmacology of the dopamine transporter: atypical inhibitors, allosteric modulators, and partial substrates. *J. Pharmacol. Exp. Ther.* **346,** 2–10 (2013).

Supplementary Information is available in the online version of the paper.

Acknowledgements We thank J. Coleman, C.-H. Lee, S. Mansoor and other Gouaux laboratory members for helpful discussions, L. Vaskalis for assistance with figures and H. Owen for help with manuscript preparation. We acknowledge the staff of the Berkeley Center for Structural Biology at the Advanced Light Source and the Northeastern Collaborative Access Team at the Advanced Photon Source for assistance with data collection. This work was supported by an NIMH Ruth Kirschstein postdoctoral fellowship and Brain and Behavior Research Foundation Young Investigator research award (K.H.W.), a postdoctoral fellowship from the American Heart Association (A.P.) and by the NIH (E.G) and the Methamphetamine Abuse Research Center of OHSU (P50DA018165 to E.G). E.G. is an investigator with the Howard Hughes Medical Institute.

Author Contributions A.P., K.H.W. and E.G. designed the project. A.P. and K.H.W. performed protein purification, crystallography and biochemical assays. A.P., K.H.W. and E.G. wrote the manuscript.

Author Information The coordinates for the structure have been deposited in the Protein Data Bank under the accession codes 4XP1, 4XP9, 4XP6, 4XPA, 4XP4, 4XP5, 4XPB, 4XPF, 4XPG, 4XPH, 4XPT (see Supplementary Table 1 for details). Reprints and permissions information is available at www.nature.com/reprints. The authors declare no competing financial interests. Readers are welcome to comment on the online version of the paper. Correspondence and requests for materials should be addressed to E.G. (gouauxe@ohsu.edu).

METHODS

Constructs. dDAT constructs employed in this study include:

subsite B mutations (sub^B). Denotes the addition of mutations D121G (TM helix 3) and S426M (TM helix 8) in the binding pocket.

dDAT$_{wt}$. Full-length dDAT without thermostabilizing mutations, fused to a C-terminal GFP tag.

dDAT$_{del}$. Contains an N-terminal deletion from 1–20 (Δ1–20) and a deletion in extracellular loop 2 (EL2) from 164–191, with thermostabilizing mutations V74A and L415A.

ts^2 dDAT$_{cryst}$. Contains thermostabilizing mutations (V74A, L415A), Δ1–20, a deletion in EL2 from Δ164–206, and a thrombin site (LVPRGS) replacing residues 602–607 (Supplementary Table 1). Structure reported of this construct with sub^B mutations in complex with cocaine and RTI-55.

ts^5 dDAT$_{cryst}$. Identical to ts^2 dDAT$_{cryst}$ except that it contains three additional thermostabilizing mutations (V275A, V311A, G538L) (Supplementary Table 1). Equivalent construct containing sub^B mutations reported for β-CFT.

dDAT$_{mfc}$. Contains thermostabilizing mutations (V74A, L415A), Δ1–20, a modified deletion in EL2, that is, Δ162–202, and a thrombin site replacing residues 602–607.(Supplementary Table 1). Structures in complex with cocaine, RTI-55, D-amphetamine, (+)-methamphetamine, DA and 3,4-dichlorophenethylamine (DCP) are reported. Structure of dDAT$_{mfc}$ containing sub^B mutations reported in complex with DCP.

dDAT$_{mfc}$ 201. Identical to dDAT$_{mfc}$ except the deletion in EL2 is from Δ162-201. (Supplementary Table 1). Structure of dDAT$_{mfc}$ 201 containing sub^B mutations reported in complex with DCP.

Expression and purification. The dDAT constructs were expressed as C-terminal green fluorescent protein (GFP)–His$_8$ fusions using baculovirus-mediated transduction of mammalian HEK-293S GnTI$^-$ cells[51,52]. Membranes harvested from cells post-infection were homogenized with 1× TBS (20 mM Tris pH 8.0, 100 mM NaCl) and solubilized with a final concentration of 20 mM *n*-dodecyl β-D-maltoside (DDM) and 4 mM cholesteryl hemisuccinate (CHS) in 1× TBS. Detergent-solubilized material was incubated with cobalt-charged metal affinity resin and eluted with 1× TBS containing 1 mM DDM and 0.2 mM CHS along with 80 mM imidazole (pH 8.0). The GFP–His$_8$ tag was removed using thrombin digestion followed by concentrating the metal ion affinity purified protein. The thrombin-digested protein was subjected to size exclusion chromatography through a Superdex 200 10/300 column pre-equilibrated with buffer containing 20 mM Tris pH 8.0, 300 mM NaCl, 4 mM decyl β-D-maltoside, 0.2 mM CHS and 0.001% (w/v) 1-palmitoyl-2-oleoyl-*sn*-glycero-3-phosphoethanolamine (POPE). Peak fractions greater than 0.5 mg ml^{-1} were collected and pooled together. Ascorbic acid (25 mM) was added to the protein solution used to crystallize the DA–dDAT$_{mfc}$ complex, to serve as antioxidant. All procedures were carried out at 4 °C.

Fab complexation and crystallization. Antibody fragment (Fab) 9D5 was used to complex with the protein at a molar ratio of 1.2 (Fab):1 (protein). The Fab–DAT complex solution was incubated with 1–2 mg solid drug for 30 min on ice followed by concentration in a 100 kDa cutoff concentrator to 3.5–5 mg ml^{-1}. The concentrated protein was spun down to remove excess drug and insoluble aggregates and plates were set up by hanging drop vapour diffusion. Crystals of Fab–DAT complex grew primarily in conditions containing PEG 400 or PEG 350 monomethyl ether or PEG 600 as the precipitant (Extended Data Table 2b). The pH range of crystallization was 8.0–9.0 for dDAT$_{cryst}$-based constructs and in the range of 6.5–8.0 with dDAT$_{mfc}$-based constructs (Extended Data Table 2b). Crystals of dDAT$_{mfc}$ were primarily obtained by streak seeding with a cat whisker dipped in crystals formed with sub^B containing constructs, 2–5 days after drops were set up. All crystals were grown at 4 °C.

Data collection and structure refinement. Crystals were directly flash-cooled in liquid nitrogen when the PEG 400 concentration in the mother liquor exceeded 36%. For crystals grown in wells containing less than 36% PEG 400, crystals were transferred into cryoprotection solution identical to the reservoir solution but with 40% PEG 400. In conditions with 30–34% PEG 600 as the primary precipitant, 10% of ethylene glycol was added to provide additional cryoprotection. Data were collected either at ALS (5.0.2; 8.2.1) or APS (24-IDC and IDE). Anomalous data for iodine containing RTI-55 complexed with dDAT was collected at 1.6 Å as described in the crystallographic data table. Data were processed using either HKL2000[52,53] or XDS[54]. Molecular replacement was carried out for all data sets using coordinates 4M48 with Fab 9D5 and dDAT$_{cryst}$ used as independent search models, using PHASER in the PHENIX software suite[55,56]. Iterative cycles of refinement and manual model building were carried out using PHENIX and COOT[57], respectively, until the models converged to acceptable levels of R-factors and stereochemistry.

Radiolabel binding and uptake assays. All binding assays were carried out by scintillation proximity assay (SPA) method[58]. Reactions contained 5–20 nM protein, 0.5 mg ml^{-1} Cu-YSi beads, SEC buffer, and [[^{3}H]nisoxetine] from 0.1 to 300 nM for saturation binding assays. Competition binding assays were done with 30 nM [^{3}H]nisoxetine and increasing concentrations of unlabelled competitor. K_i values were estimated from IC_{50} values using the Cheng–Prusoff equation. Fits were plotted using Graphpad Prism v4.0.

For uptake assays HEK 293S cells were infected with baculovirus expressing dDAT$_{mfc}$ or dDAT$_{wt}$, and sodium butyrate was added to 10 mM 8–12 h post-infection. At 24 h, infected cells were adhered to Cytostar-T plates for 2 h, after which the culture media were replaced with uptake buffer (20 mM HEPES pH 7.4, 120 mM NaCl, 5 mM KCl, 2.5 mM $CaCl_2$, 1.2 mM $MgSO_4$, 10 mM D-glucose, 1 mM tropolone, 1 mM L-ascorbic acid[59,60]. Uptake assays were carried out using [^{14}C]DA over a range of 0.3–60 μM in 100 μl total volume. Samples were read every five minutes for a time course over twenty-five minutes. The linear initial rate of uptake was plotted in the presence and absence of 10 μM nortriptyline to calculate the specific uptake rate. Data were fitted to a standard Michaelis–Menten equation to obtain K_M and V_{max} values. The significance of specific uptake was assessed at each concentration of DA using a two-tailed Welch's *t*-test with 2 degrees of freedom.

51. Reeves, P. J., Callewaert, N., Contreras, R. & Khorana, H. G. Structure and function in rhodopsin: high-level expression of rhodopsin with restricted and homogeneous N-glycosylation by a tetracycline-inducible N-acetylglucosaminyltransferase I-negative HEK293S stable mammalian cell line. *Proc. Natl Acad. Sci. USA* **99,** 13419–13424 (2002).
52. Goehring, A. *et al.* Screening and large-scale expression of membrane proteins in mammalian cells for structural studies. *Nature Protocols* **9,** 2574–2585 (2014).
53. Otwinowski, Z., &. Minor, W. Processing of X-ray diffraction data collected in oscillation mode. *Methods Enzymol.* **276,** 307–326 (1997).
54. Kabsch, W. XDS. *Acta Crystallogr. D* **66,** 125–132 (2010).
55. McCoy, A. J. *et al.* Phaser crystallographic software. *J. Appl. Crystallogr.* **40,** 658–674 (2007).
56. Afonine, P. V. *et al.* Towards automated crystallographic structure refinement with phenix.refine. *Acta Crystallogr. D* **68,** 352–367 (2012).
57. Emsley, P. & Cowtan, K. Coot: model-building tools for molecular graphics. *Acta Crystallogr. D* **60,** 2126–2132 (2004).
58. Quick, M. & Javitch, J. A. Monitoring the function of membrane transport proteins in detergent-solubilized form. *Proc. Natl Acad. Sci. USA* **104,** 3603–3608 (2007).
59. Eshleman, A. J. *et al.* Metabolism of catecholamines by catechol-*O*-methyltransferase in cells expressing recombinant catecholamine transporters. *J. Neurochem.* **69,** 1459–1466 (1997).
60. Dehnes, Y. *et al.* Conformational changes in dopamine transporter intracellular regions upon cocaine binding and dopamine translocation. *Neurochem. Int.* **73,** 4–15 (2014).

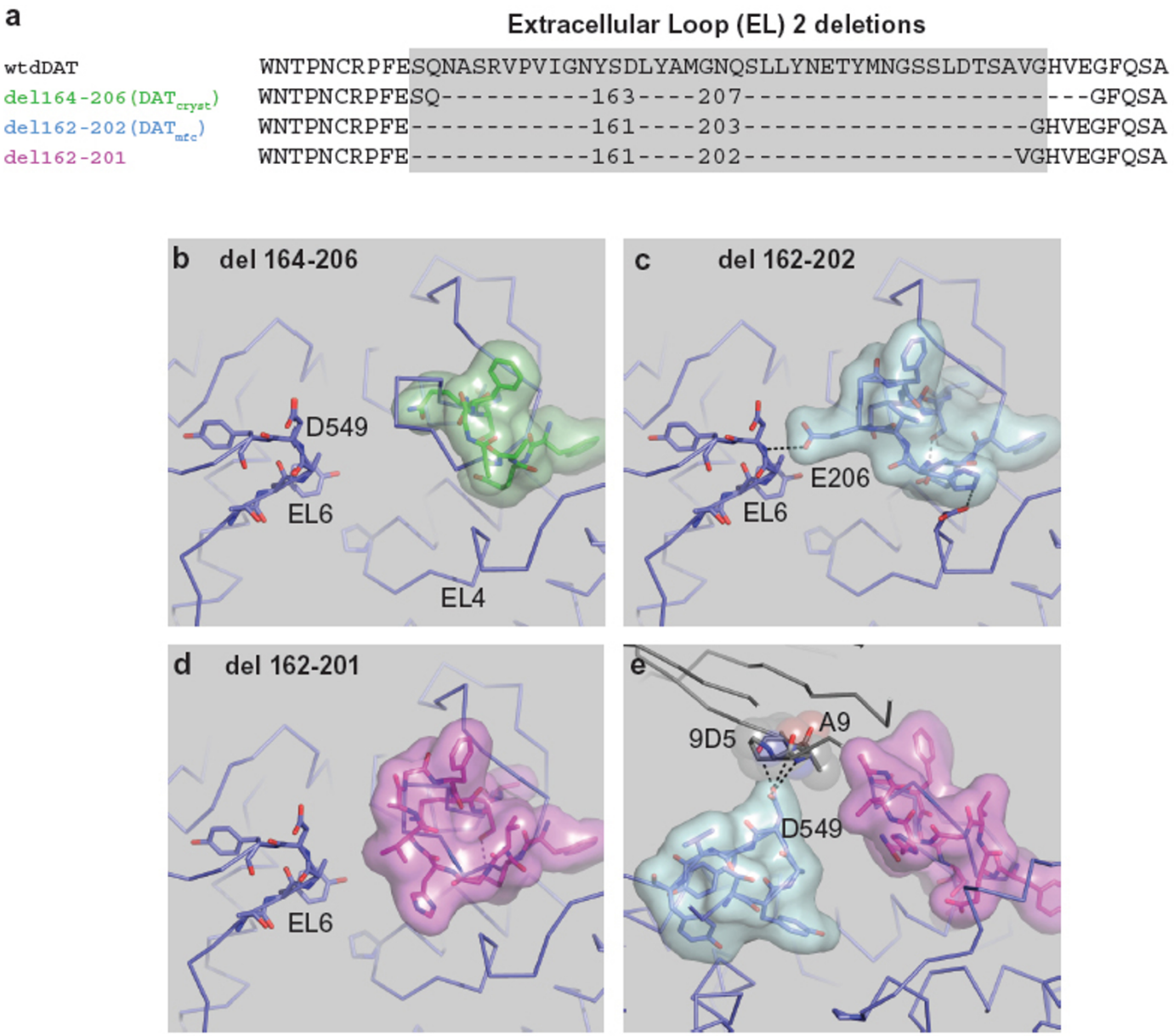

Extended Data Figure 1 | Design of the minimal functional construct. **a**, Thermostabilizing (ts) mutations V275A, V311A, G538L were removed. Modification of the EL2 deletion from 164–206 to 162–202, which recovered transport activity. The del 162–201 construct has robust dopamine uptake activity. **b**, Structural organization of EL2 regions. Organization of dDAT$_{cryst}$ with a deletion of region 164–206 depicted as green surface. **c**, EL2 structure in dDAT$_{mfc}$ with the deletion 162–202 depicted as cyan surface showing contacts between EL2 and EL6. **d**, EL2 organization in the construct with a deletion from 162–201 depicted as magenta surface. **e**, Fab 9D5 interferes with the interaction between EL2 and EL6 in the crystal lattice, with loops depicted as magenta and cyan surfaces, respectively. Fab disrupts the EL organization in all structures. The del 162–201 sub^{B} structure is shown.

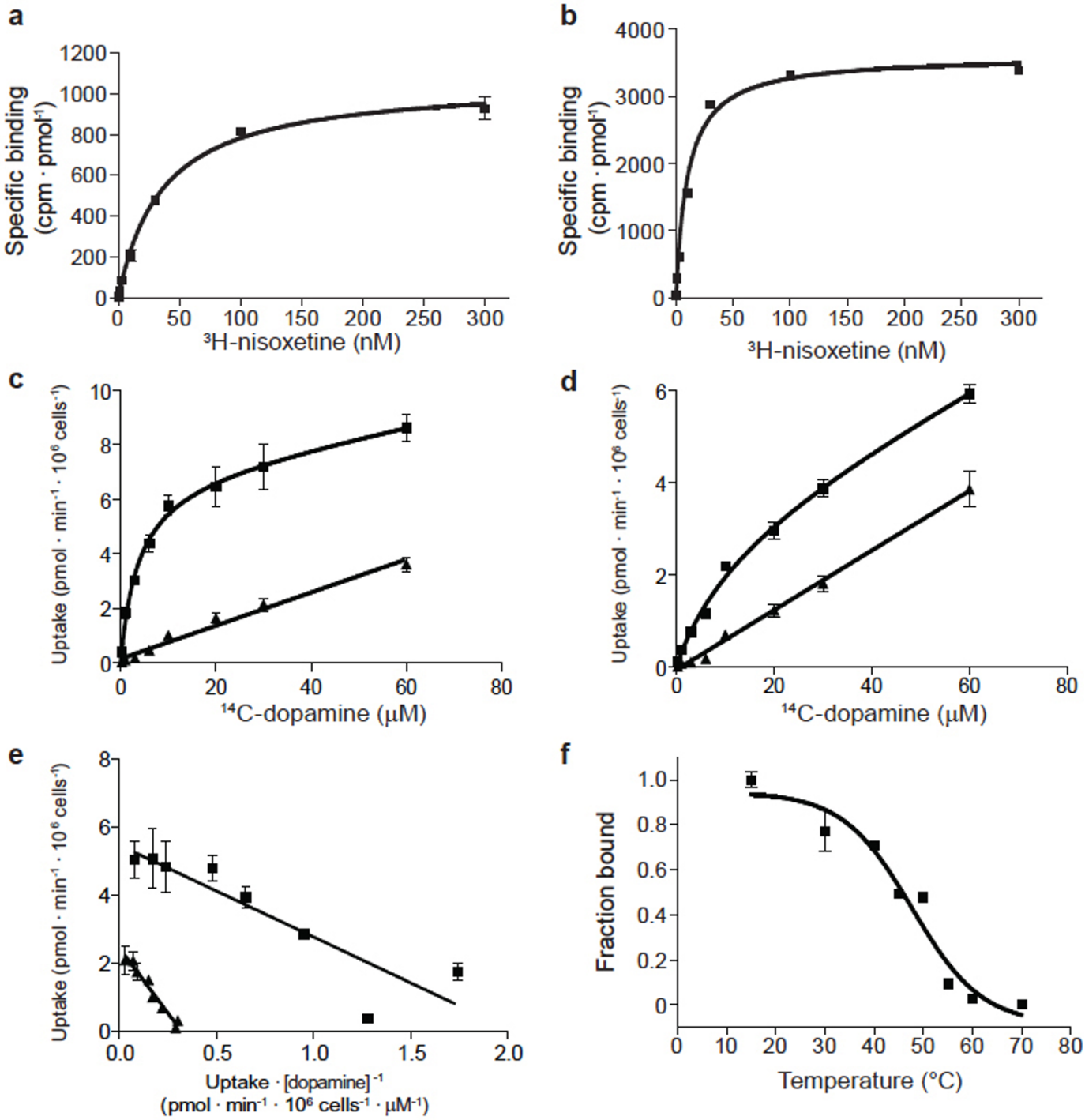

Extended Data Figure 2 | Measurement of dissociation constants using purified dDATmfc protein, and dopamine uptake in whole cells. **a**, $dDAT_{mfc}$ binds [^{3}H]nisoxetine with a K_d of 36 ± 3 nM (s.e.m.). **b**, $dDAT_{mfc}$ with sub^B mutations binds [^{3}H]nisoxetine with a K_d of 10 ± 1 nM (s.e.m.). **c**, **d**, Michaelis–Menten plots of [^{14}C]dopamine uptake by HEK293S cells expressing $dDAT_{wt}$ or $dDAT_{mfc}$, respectively, which yielded a K_M of 2.1 ± 0.7 μM and V_{max} of 4.5 ± 0.4 pmol min^{-1} per 10^6 cells for $dDAT_{wt}$ and a K_M of 8.2 ± 2.3 μM and V_{max} of 2.4 ± 0.2 pmol min^{-1} per 10^6 cells for $dDAT_{mfc}$ (s.e.m.). One representative plot of total and background counts (in the presence of 10 μM nortriptyline) is shown of two experimental trials as squares and triangles, respectively. Data points and error bars show the average and standard deviation, respectively, of technical replicates (n = 3). Welch's *t*-test indicates that the specific uptake signal at each concentration of dopamine is significant with a two-tailed P value < 0.02. **e**, Eadie–Hofstee plot of specific dopamine uptake shown in Fig. 1a and panels **c** and **d** of this figure. Data for $dDAT_{wt}$ and $dDAT_{mfc}$ are shown as squares and triangles, respectively, and error bars denote s.d. of technical replicates (n = 3). **f**, The thermal melting curve of $dDAT_{mfc}$ solubilized from HEK293S membranes in the presence of 100 nM [^{3}H]nisoxetine exhibits a melting temperature of 48 ± 2 °C (s.e.m.). The fraction bound describes the signal remaining after incubation at the specified temperature for 10 min, normalized to the signal at 4 °C. Data points show the mean values for one experimental trial, and error bars show the s.d. of technical replicates (n = 3).

a **Locations of Subsite B mutations**

```
                  D121G (TM3)          S426M (TM8)
dDAT 116-IAFYVDFYYNV-126 421-SSFGGSEAIITALSD-435
hDAT 148-ISLYVGFFYNV-158 422-SAMGGMESVITGLID-436
hNET 144-IALYVGFYYNV-154 419-SSMGGMEAVITGLAD-433
hSERT168-IAFYIASYYNT-178 438-STFAGLEGVITAVLD-452
```

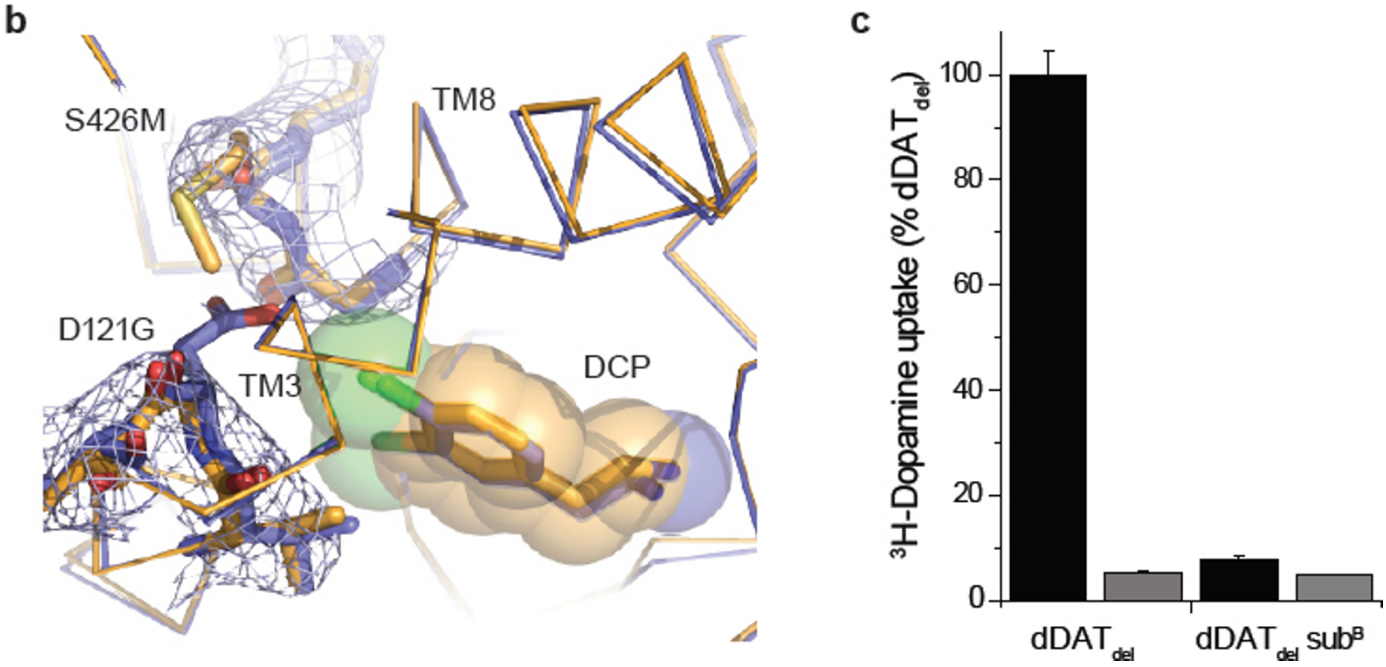

Extended Data Figure 3 | Mutagenesis and effects of DAT subsite B. **a**, Sequence alignment of subsite B regions for dDAT and human NSS orthologues. **b**, $2F_o - F_c$ density contoured at 0.9σ around the vicinity of the D121G (TM3) and S426M mutations (TM8). **c**, Abrogation of dopamine transport activity by $dDAT_{wt}$ bearing both subsite B mutations in infected HEK293S cells. Data show the average uptake and error bars show the data range of technical duplicates for a single trial. Reactions were performed without and with 100 μM desipramine in black and grey bars, respectively.

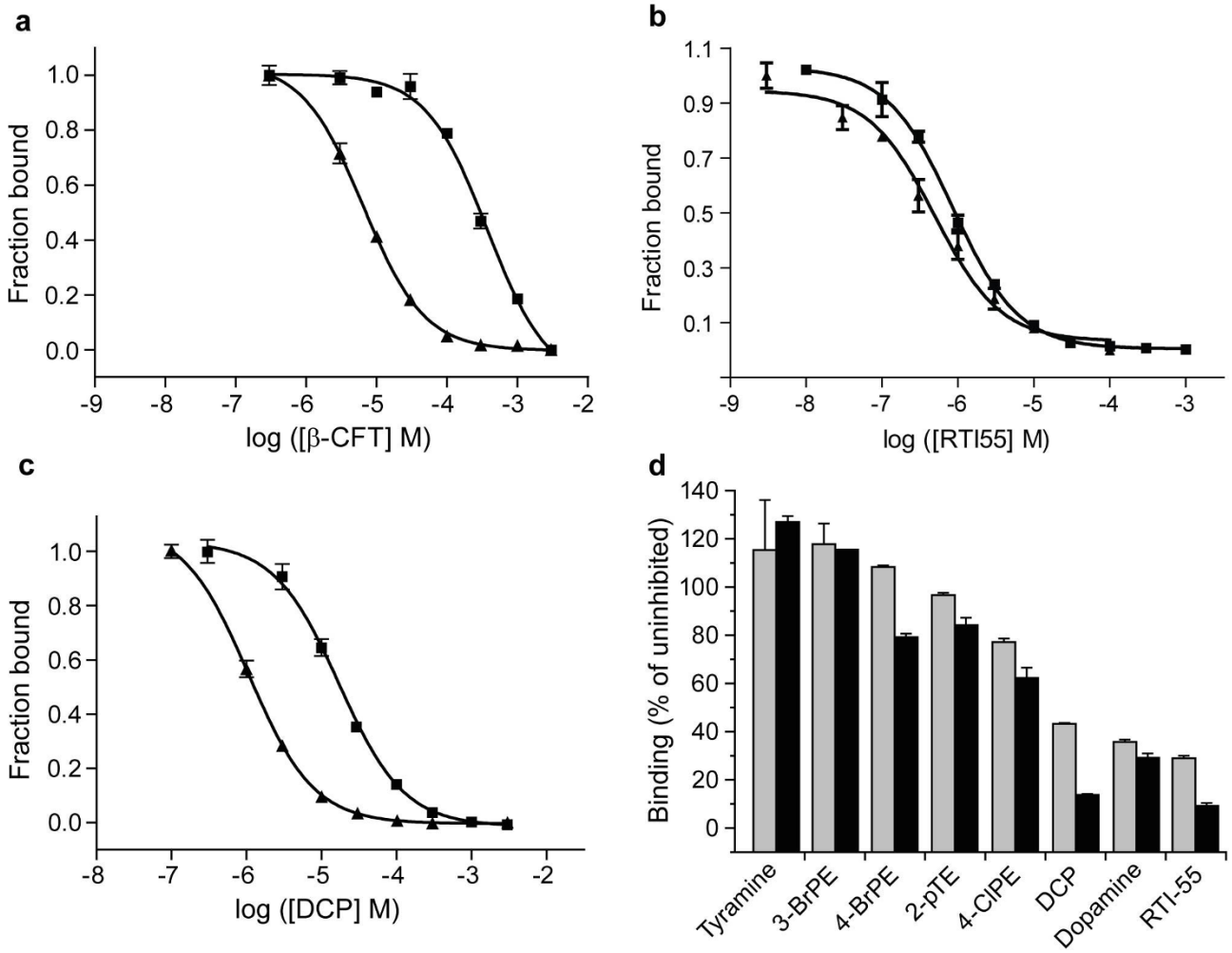

Extended Data Figure 4 | Measurement of inhibition constants using purified dDAT protein. **a–c**, Inhibition of [^{3}H]nisoxetine binding to $dDAT_{mfc}$ (squares) and $dDAT_{mfc}$ sub^B (triangles). K_i inhibition constants for $dDAT_{mfc}$ and $dDAT_{mfc}$ sub^B are, respectively, 98 ± 4 μM, and 1.4 ± 0.1 μM, (**a**, β-CFT), 371 ± 25 nM and 271 ± 59 nM (**b**, RTI-55), and 4.5 ± 0.3 μM, and 267 ± 20 nM (**c**, DCP). All errors are s.e.m. One representative trial of two is shown for all experiments in panels **a–c**, and data points and error bars denote the average values for fraction bound and standard deviation, respectively, for technical replicates ($n = 3$). **d**, Inhibition of [^{3}H]nisoxetine (50 nM) binding to $dDAT_{del}$ by 1 and 10 μM unlabelled compound (grey and black bars, respectively). Error bars show the data range of technical replicates ($n = 2$). Abbreviations: 3-BrPE, 3-bromophenethylamine; 4-BrPE, 4-bromophenethylamine; 2-pTE, 2-(pTolyl)ethylamine, 4-ClPE, 4-chlorophenethylamine; DCP, 3,4-dichlorophenethylamine.

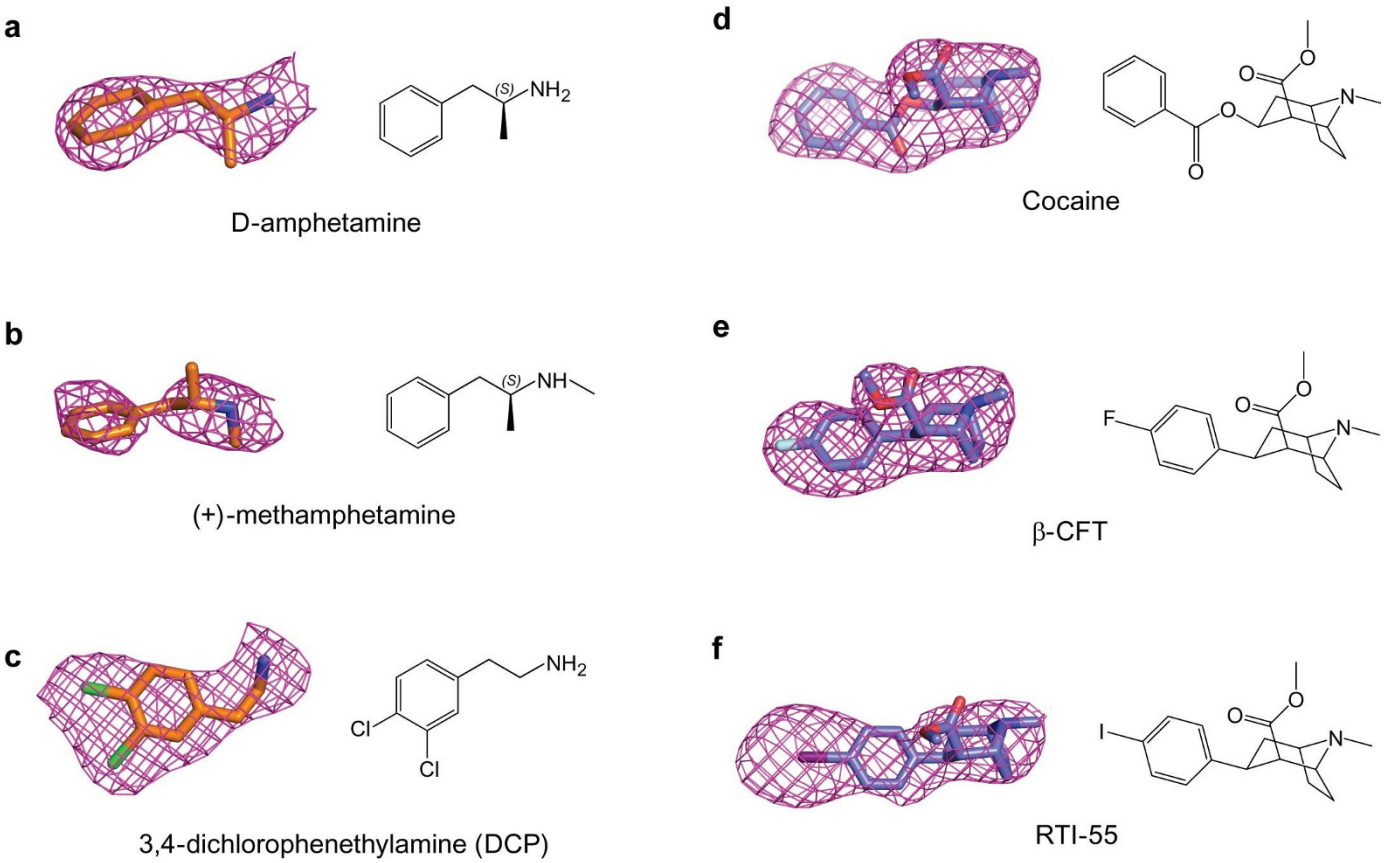

Extended Data Figure 5 | $F_o - F_c$ densities for ligands complexed with dDAT. **a**, D-amphetamine (2.4σ); **b**, (+)-methamphetamine (1.8σ); **c**, DCP (2.2σ); **d**, cocaine (2.2σ); **e**, β-CFT (2.2σ); **f**, RTI-55 (2.6σ).

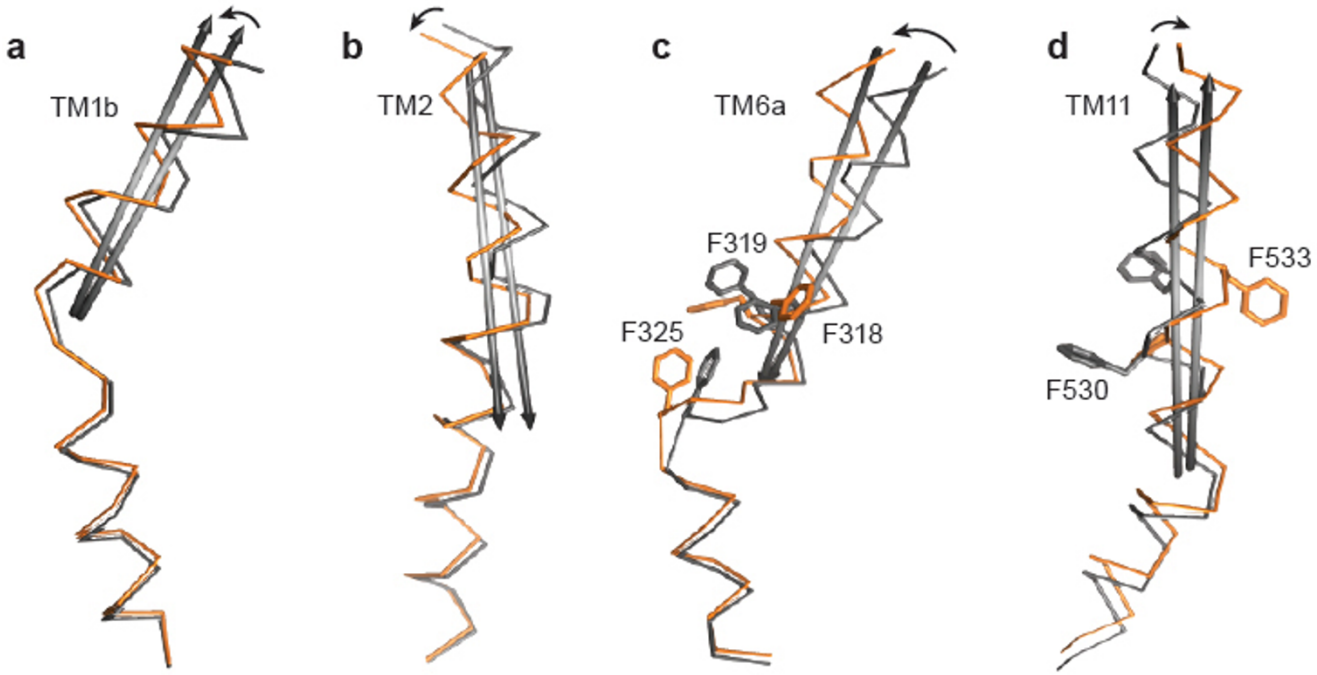

e

Motif	dDAT (°)	LeuT (°)
TM1b	+ 5.6	+ 9.2
TM2	+ 3.7	+ 8.7
TM6a	+ 7.2	+ 5.5
TM11	– 4.0	– 5.9

+/– indicates inward or outward helical movements.

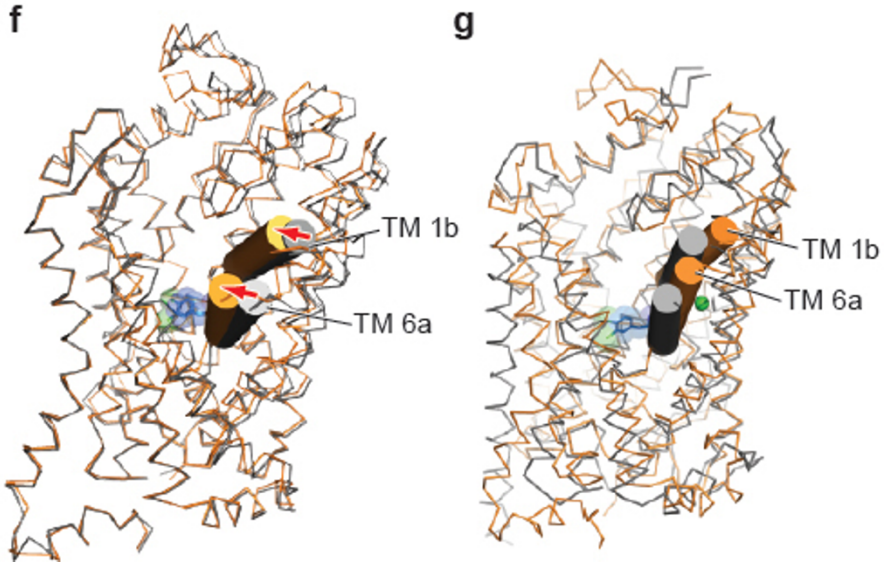

Extended Data Figure 6 | Helical movements in dDAT$_{mfc}$ upon binding to substrate analogue DCP (orange) and inhibitor nortriptyline (grey). **a**–**d**, Helices undergoing maximal shifts are **a**, TM1b; **b**, TM2; **c**, TM6a; **d**, TM11. Arrows in black represent direction of shift. **e**, Table comparing angular shifts between nortriptyline–dDAT$_{cryst}$ (PDB ID 4M48) and DCP–dDAT$_{mfc}$ structures in column one, and between the outward-open Trp–LeuT (PDB ID 3F3A) and outward-occluded Leu–LeuT (PDB ID 2A65) structures in column two. **f**, Superposition of the outward open state of nortriptyline–dDAT$_{cryst}$ (PDB ID 4M48) and DCP–dDAT$_{mfc}$ structures in grey and orange ribbon, respectively. Extracellular gating TMs 1b and 6a are shown as cylinders. Arrows in red indicate inward movement of TMs 1b and 6a. **g**, Superposition of the occluded state of LeuT (PDB ID 2A65) and DCP–dDAT$_{mfc}$ structures in grey and orange ribbon, respectively.

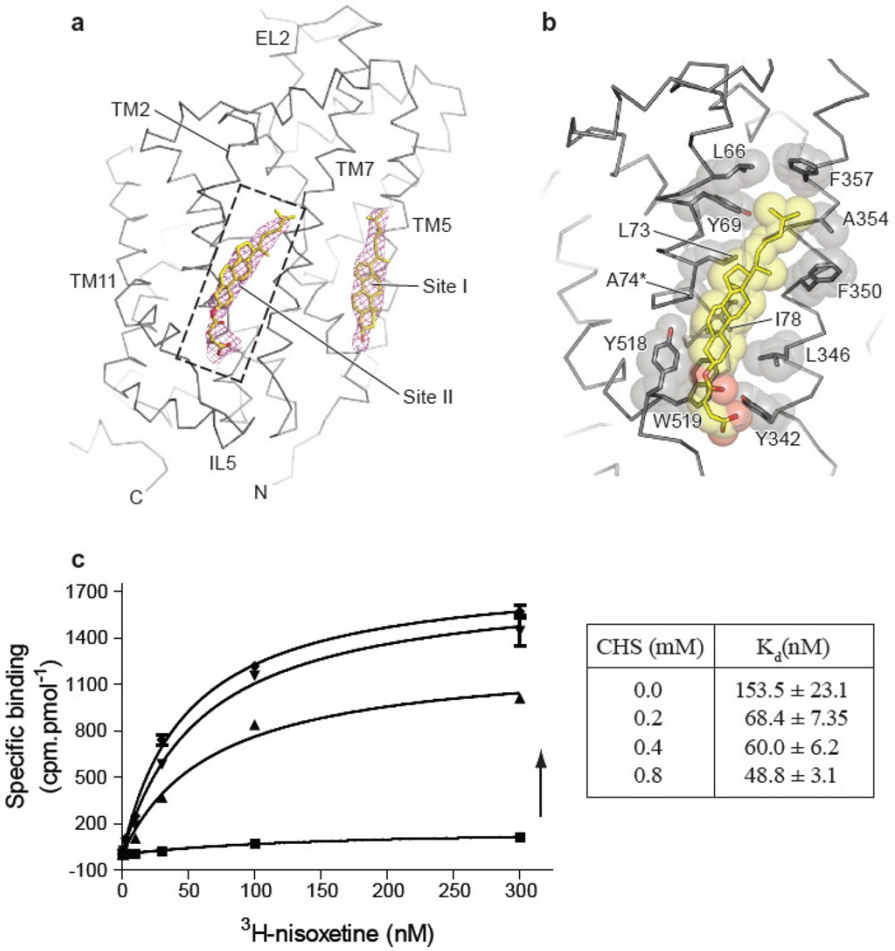

CHS (mM)	K_d(nM)
0.0	153.5 ± 23.1
0.2	68.4 ± 7.35
0.4	60.0 ± 6.2
0.8	48.8 ± 3.1

Extended Data Figure 7 | Cholesterol binding sites in DAT. **a**, Cholesterol binding sites seen on the dDAT surface corresponding to the inner leaflet of the plasma membrane, with a second novel cholesterol site into which a cholesteryl hemisuccinate (CHS) could be modelled. $F_o - F_c$ densities for cholesterol contoured at 2.0σ. **b**, Close-up view of cholesterol site II at the junction of TM2, TM7 and TM11 interacting with multiple hydrophobic residues. Asterisk denotes thermostabilizing mutant V74A. **c**, Effect of CHS concentration on [^{3}H]nisoxetine binding to DAT_{mfc} construct. Graph depicts one representative trial of two independent experiments, and total and background counts were measured using technical replicates ($n = 3$) for each binding curve at each CHS concentration. Arrow represents increasing concentration of CHS. Error bars represent s.d.

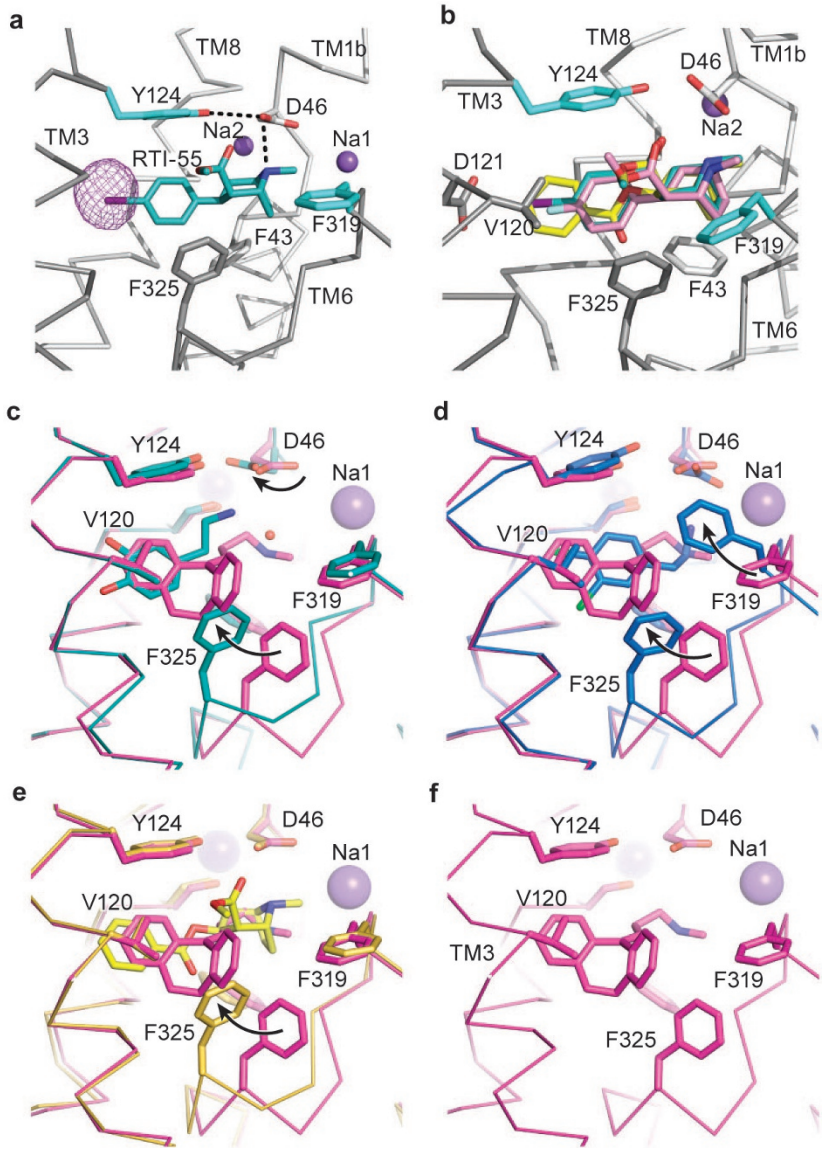

Extended Data Figure 8 | Analogues of cocaine and binding site comparisons. a, The position of RTI-55 in the binding pocket with anomalous difference density for iodide displayed as purple mesh and contoured at 4σ. **b**, Superposition of cocaine, β-CFT, and RTI-55 using the RTI-55-dDAT$_{mfc}$ structure. Ligands are shown as sticks and coloured yellow (cocaine), pink (β-CFT), and teal (RTI-55). Sodium ions are shown as purple spheres. **c**–**f**, Residues that line the binding pocket are superposed between the nortriptyline–dDAT$_{cryst}$ (magenta, PDB ID 4M48) and those of **c**, DA–dDAT$_{mfc}$ (cyan), **d**, DCP–dDAT$_{mfc}$ (marine), **e**, cocaine–dDAT$_{mfc}$ (yellow). **f**, Organization of S1 binding site in complex with nortriptyline (PDB ID 4M48). Black arrows describe the change in rotamers and positions of D46, F319, and F325 compared to the nortriptyline-bound structure.

Extended Data Table 1 | Superposition statistics of dDAT structures

	ntt ts^5 dDAT$_{cryst}$	cocaine dDAT$_{mfc}$	β-CFT ts^5 dDAT$_{cryst}$ sub^B	RTI-55 dDAT$_{mfc}$ sub^B	RTI-55 dDAT$_{mfc}$	DCP dDAT$_{mfc}$ sub^B	DCP dDAT$_{mfc}$	DA dDAT$_{mfc}$	meth dDAT$_{mfc}$	amph dDAT$_{mfc}$
ntt ts^5 dDAT$_{cryst}$	—	0.46	0.37	0.52	0.70	0.74	0.76	0.53	0.53	0.48
cocaine dDAT$_{mfc}$		—	0.27	0.46	0.67	0.74	0.79	0.52	0.54	0.37
β-CFT ts^5 dDAT$_{cryst}$ sub^B			—	0.43	0.64	0.70	0.73	0.50	0.50	0.52
RTI-55 ts^2 dDAT$_{cryst}$ sub^B				—	0.73	0.75	0.82	0.55	0.59	0.60
RTI-55 dDAT$_{mfc}$					—	0.83	0.64	0.97	0.53	0.58
DCP dDAT$_{mfc}$ sub^B						—	0.41	0.75	0.57	0.61
DCP dDAT$_{mfc}$							—	0.64	0.64	0.63
DA dDAT$_{mfc}$								—	0.64	0.41
meth dDAT$_{mfc}$									—	0.35
amph dDAT$_{mfc}$										—

Extended Data Table 2 | a, Ligand surface and interface areas*; b, crystallization conditions for ligand–DAT complexes

a

Ligand	Total surface area (Å^2)	Buried Surface area (Å^2)	% Buried
Nortriptyline (4M48)	475.9	448.4	94.2
Cocaine	484.7	447	92.2
RTI-55	466.2	416.7	89.4
β-CFT	439.2	403.1	91.8
dopamine	311.9	279.1	89.5
DCP	337.3	321.5	95.3
methamphetamine	325.7	301	92.4
D-amphetamine	308.3	284.5	92.3

b

	Ligand	Construct	Condition
1	Cocaine	$dDAT_{mfc}$	PEG 400 37%, Na MES pH 6.8 (0.1M)
2	RTI-55	$dDAT_{mfc}$	PEG 400 41%, Tris pH 8.0 (0.1M)
3	Methamphetamine	$dDAT_{mfc}$	PEG 400 38%, Tris pH 8.0 (0.1M)
4	D-amphetamine	$dDAT_{mfc}$	PEG 600 36%, MOPS pH 7.0 (0.1M)
5	DA (dopamine)	$dDAT_{mfc}$	PEG 600 31%, Tris pH 8.0 (0.1M)
6	DCP	$dDAT_{mfc}$	PEG 400 38%, Tris pH 8.0 (0.1M)
7	Cocaine	$dDAT_{cryst}\,ts^2\,sub^B$	PEG 400 38%, Tris-Bicine pH 8.5 (0.1M)
8	RTI-55	$dDAT_{cryst}\,ts^2\,sub^B$	PEG 400 39%, Bicine pH 8.8 (0.1M)
9	β-CFT	$dDAT_{cryst}\,sub^B$	PEG 400 38%, Bicine pH 8.8 (0.1M)
10	DCP	$dDAT_{mfc}\,sub^B$	PEG 400 33%, Na MES pH 6.5 (0.1M)
11	DCP	$dDAT_{mfc}\,201\,sub^B$	PEG400 34%, Na MES pH 6.5 (0.1M)

*Surface areas calculated by PDBePISA. (http://www.ebi.ac.uk/pdbe/pisa)